Directed self-assembly of silica nanoparticles in ionic liquid-spun cellulose fibers

Journal of Colloid and Interface Science 553 (2019) 167–176

Contents lists available at ScienceDirect

Journal of Colloid and Interface Science

journal homepage: www.elsevier.com/locate/jcis

Regular Article

Directed self-assembly of silica nanoparticles in ionic liquid-spun cellulose fibers

Markus Andersson Trojer [a,*], Carina Olsson [a], Jenny Bengtsson [b], Arthur Hedlund [b], Romain Bordes [c]

[a] Department of Materials, Bio-based fibres, RISE IVF, 431 53 Mölndal, Sweden
[b] Department of Chemistry and Chemical Engineering, Forest Products and Chemical Engineering, Chalmers University of Technology, 412 96 Göteborg, Sweden
[c] Department of Chemistry and Chemical Engineering, Applied Surface Chemistry, Chalmers University of Technology, 412 96 Göteborg, Sweden

GRAPHICAL ABSTRACT

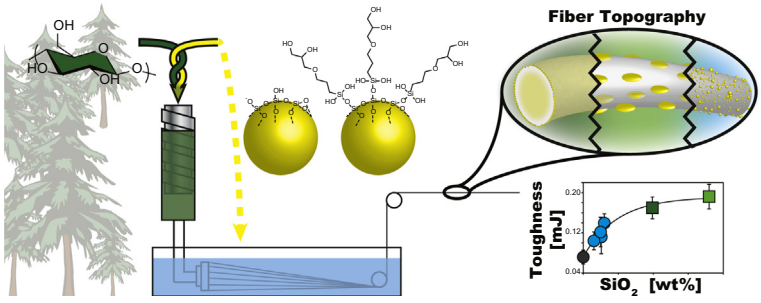

ARTICLE INFO

Article history:
Received 12 February 2019
Revised 1 May 2019
Accepted 25 May 2019
Available online 25 May 2019

Keywords:
Wet-spinning
Biocomposites
Mechanical properties
Surface topography
Plasma-enhanced chemical vapor deposition

ABSTRACT

The application range of man-made cellulosic fibers is limited by the absence of cost- and manufacturing-efficient strategies for anisotropic hierarchical functionalization. Overcoming these bottlenecks is therefore pivotal in the pursuit of a future bio-based economy. Here, we demonstrate that colloidal silica nanoparticles (NPs), which are cheap, biocompatible and easy to chemically modify, enable the control of the cross-sectional morphology and surface topography of ionic liquid-spun cellulose fibers. These properties are tailored by the silica NPs' surface chemistry and their entry point during the wet-spinning process (dope solution $^{D}SiO_2$ or coagulation bath $^{C}SiO_2$). For $^{C}SiO_2$-modified fibers, the coagulation mitigator dimethylsulphoxide allows for controlling the surface topography and the amalgamation of the silica NPs into the fiber matrix. For dope-modified fibers, we hypothesize that cellulose chains act as seeds for directed silica NP self-assembly. This results for $^{D}SiO_2$ in discrete micron-sized rods, homogeneously distributed throughout the fiber and for glycidoxy-surface modified $^{D}SiO_2$@GLYEO in nano-sized surface aggregates and a cross-sectional core-shell fiber morphology. Furthermore, the dope-modified fibers display outstanding strength and toughness, which are both characteristic features of biological biocomposites.

1. Introduction

The interest in man-made cellulosic fibers - as an alternative to conventional fibers, in particular cotton – has steadily increased since the invention of the viscose process a century ago. Cellulosic fibers and the associated products are capitalizing on the mechanical and physicochemical features of this abundant polysaccharide

* Corresponding author at: RISE IVF, Department of materials, Division of bio-based fibres, Argongatan 30, 431 53 Mölndal, Sweden.
E-mail address: markus.andersson-trojer@ri.se (M. Andersson Trojer).

https://doi.org/10.1016/j.jcis.2019.05.084
0021-9797/

[1,2]. However, the production of cellulose fibers *via* wet-spinning by traditional methods such as chemical derivatization (e.g. the viscose process) is chemical and energy exhaustive and consequently environmentally harmful despite the abundance and the renewable biodegradable nature of cellulose. In addition, the quality of the resulting fibers are far from that of cotton [3]. Yet, the recent advent of ionic liquids has significantly expanded the range of green environmentally friendly processes for cellulose dissolution and spinning [3–6]. But this progress is not sufficient and in order to realize a future bio-based circular economy - in which cellulose will play a pivotal role as raw material - it is essential to broaden its application spectrum through a wider set of properties. There is therefore a need for new strategies to chemically modify and to mechanically alter wet-spun cellulose fibers. In that sense, bio-mimicking anisotropic functionalization on different hierarchical length scales is desirable in order to enable e.g. self-cleaning properties, directional and/or region-specific interactions, self-assembly processes, etc [7–10]. As means for functionalization and (chemical) modification, silica nanoparticles (NP) are very attractive candidates. Silica is an inorganic, biocompatible and environmentally benign material which similar to cellulose is abundant, cheap but also very versatile in terms of mineralization and formation [11–16]. Additionally, silica can conveniently be chemically functionalized using e.g. well-established silane-based condensation reactions [16–18]. In Nature, siliceous components are used for protection and stability, e.g. in sponge spicules, in the diatom frustule, as phytolites in plants and in the radular teeth of the limpet [8,14]. Improved mechanical stability, in particular high toughness (such as in bone), is the usual feature of biocomposites where macromolecules (polysaccharides or proteins) guide the biomineralization of the inorganic material [8,14,19].

Inspired by such material, we demonstrate here three different ways for controlling the particle growth/aggregation, morphology and surface topography of wet-spun silica-cellulose composite fibers *in-situ* using a bench scale multifilament solution spinning equipment (Scheme 1). The aforementioned properties are conveniently tailored by the surface chemistry of the colloidal silica as well as its entry point during the wet-spinning process. The considerable majority of research on siliceous cellulose composite fibers has been investigated within the scope of the excellent flame-retardancy provided by silica [20]. Most strategies rely on post-modification of viscose-produced cellulose fibers or by introducing silica precursor in the viscose process under the form of alkoxysilanes [21,22]. This is the first publication which combines the unique gelling behavior of colloidal silica in ionic liquids [6] and the wet-spinning of cellulose fibers from mixtures of the same. The focus of this work is - in addition to the hierarchical and anisotropic composite structure of and particle distribution in the cellulose fibers - on the material and surface properties of this novel class of composite fiber which display a considerable strength and in particular toughness improvement over the native cellulose filaments.

2. Experimental

2.1. Materials

The cellulose pulp (Buckeye, GP Cellulose GmbH, Zug, CH) was of 95% α-cellulose purity (see Table S1 in the Supplementary

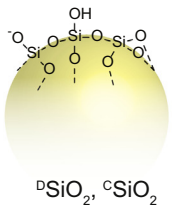

Silica type	μ [nm]	σ [nm]	Surface groups
$^{D}SiO_2$	12	~0	-O^-, OH
$^{D}SiO_2$@GLYEO	12	~0	GLYEO
$^{C}SiO_2$	60	15	-O^-, OH

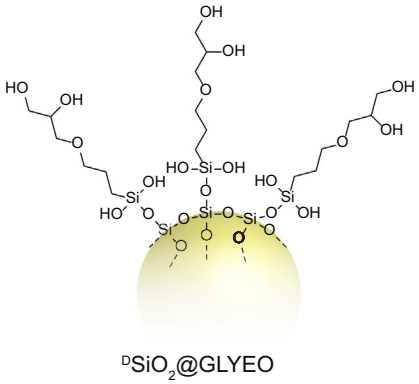

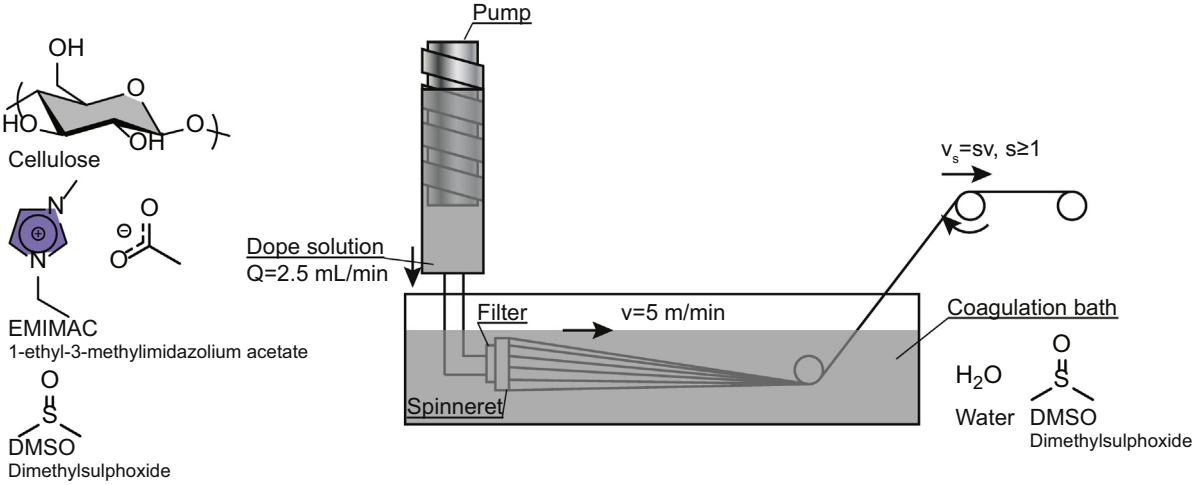

Scheme 1. The wet-spinning setup including the dope and coagulation bath composition. The mean size μ (diameter) and standard deviation σ of the colloidal silica was determined using dynamic light scattering and the Contin algorithm as presented in the Supplementary material. The superscripts "D" and "C" denotes "dope solution" and "coagulation bath", respectively.

material). Ethylmethylimidazolium acetate (EMIMAC), dimethylsulphoxide (DMSO) and trimethoxypropylsilane ($(MeO)_3PrSi$) were of analytical grade (Sigma Aldrich Sweden, Stockholm, SE). Distilled water was used for all water samples. Amorphous colloidal silica; unmodified Bindzil 40/220 $^{D}SiO_2$ (50 wt%, monodisperse), surface modified Levasil cc301 with 3-(2,3-epoxypropoxy)propyl triethoxysilane (GLYEO) $^{D}SiO_2$@GLYEO (30 wt%, monodisperse) and unmodified Bindzil 50/80, $^{C}SiO_2$ (50 wt%, polydisperse) were obtained from Nouryon (Bohus, SE).

2.2. Wet-spinning

Cellulose filaments were spun using a bench scale multifilament solution spinning equipment, with in-line filtration through a 5 μm sintered nonwoven stainless steel filter. The solution was extruded at ambient temperature through a spinneret with 64 capillaries with the diameter of 100 μm. The extrusion rate Q was fixed at 2.5 ml min^{-1}, resulting in a filament extrusion speed v of 5 m min^{-1}. The take-up speed v_s was also fixed at 5 m min^{-1} to give filaments with a stretch ratio $s = 1$ in order to allow for the investigation of the effect of silica modification in the absence of additional alignment/orientation effects. The extruded filaments were precipitated in water or in water/DMSO mixtures at room temperature (see below). The fibers were collected immediately after the coagulation bath, as described in Scheme 1, and subsequently washed thoroughly in distilled water and dried at constant length at room temperature for 24 h. Prior to mechanical testing and birefringence analysis, filaments were conditioned at 65 ± 2% relative humidity and 20 ± 2 °C for at least 24 h.

2.2.1. Silica in dope solution

For the silica, $^{D}SiO_2$ or $^{D}SiO_2$@GLYEO, added to the dope solutions, 0.5 wt% silica (representing 10 wt% of the solid fiber content) was added from a concentrated suspension to the already dissolved pulp. $^{D}SiO_2$ which aggregates in the presence of cellulose was allowed to gel at 70 °C for 24 h during the degassing procedure in accordance with general dissolution procedure as described in the Supplementary material.

2.2.2. Silica in coagulation bath

1 wt% $^{C}SiO_2$ was added to the coagulation bath under gentle stirring. In order to assess the effect of the coagulation rate, filaments were extruded into suspension containing various amounts of DMSO (0, 4, 12 and 36 wt%).

2.3. Birefringence

The birefringence Δn (Eqs. (1) and (2) - where n_o is the ordinary and n_e is the extraordinary refractive index, R is the retardation and D is the filament diameter - and the subsequent semi-empirical orientation factor f (Eq. (3)) of the filaments were measured using optical microscopy (Nikon Eclipse Ci-Pol, Brighton, MI, US) with a supplemental Berek compensator (Nishika Co., Kyoto, J). For each type of modification, the obtained Δn and f was estimated from the mean of at least 10 filaments.

$$|n_e - n_o| = \Delta n \tag{1}$$

$$R = D \cdot \Delta n \tag{2}$$

$$\Delta n = f \cdot \Delta n_{max} \tag{3}$$

The retardation was obtained directly by the tilt angle φ of the Berek compensator according to Fig. S4 in the Supplementary material. Δn_{max} in Eq. (3) was 0.062 as obtained using the Lenz formalism [23].

2.4. SEM

The fibers were mounted on a SEM stub using a silver adhesive and sputtered with a 1 nm or 1.5 nm thin platina layer for the cross-sectioned or top-viewed samples respectively. The samples were analysed using a high-resolution SEM (JEOL JSM-7800F, JEOL, Peabody, US) operating at an accelerating voltage of 5 kV. The working distance was 4 mm for the microscopy and 10 mm for the EDS analysis.

2.4.1. Cross-sections

Samples for cross-section analyses were prepared by vacuum impregnation and cold mounting in epoxy. The impregnated samples were subsequently ion etched by BIB (Broad Ion Beam milling) using a Gatan Ilion (5 kV in liquid N_2 at −80 °C) and PIPS (Precision Ion Polishing System, Gatan, Pleasanton, US).

2.4.2. EDS

EDS analysis was performed using a XFlash 5020 detector (Bruker, Billerica, US). Quantification by mapping and line analysis were performed at 5 kV accelerating voltage, 10–11 kc/s for 10 min.

2.5. Fiber density

The density of the fiber ρ was determined by detecting its fundamental resonance frequency, induced by mechanical oscillation using a Vibroscope (Vibroskop, Lenzing Technik GmbH & Co KG) operating at frequency $f = 2.0$ MHz. The resonance condition for the fundamental frequency is described in Eq. (4).

$$\rho = \frac{F(2lf)^{-2}(1+\Delta)}{\pi r^2} \tag{4}$$

$$\lambda = \rho \pi r^2 \tag{5}$$

$$\Delta = 2\alpha + 5.47\alpha^2 + \cdots \tag{6}$$

$$\alpha = \frac{4EI}{l^2 F} \tag{7}$$

$$I = \frac{\pi r^4}{4} \tag{8}$$

The nonlinear correction factor Δ which takes the form of a geometric sum (Eq. (6)) accounting for the stiffness of the fiber E (as described by the factor α in Eq. (7)) was minimized by maximizing the tension weight F and the length. The resonance was induced at a fixed mechanical oscillating frequency by varying l. The radii of the fibers were obtained from SEM measurements. λ in Eq. (5) is the linear fiber density.

2.5.1. Estimation of silica concentration

The silica concentration in the fiber was estimated using the measured fiber density from mechanical oscillation (Eq. (4)) and from the fiber radii from SEM according to Eq. (9) where w_{SiO2} and $w_{Cellulose}$, ρ_{SiO2} (2.65 g/cm^3) and $\rho_{Cellulose}$ (1.50 g/cm^3) are the weight fractions and densities of silica and cellulose respectively.

$$\begin{aligned} w_{SiO_2}\rho_{SiO_2} + w_{\ Cellulose}\ \rho_{\ Cellulose} &= \rho \\ w_{Cellulose} &= 1 - w_{SiO_2} \end{aligned} \tag{9}$$

Eq. (9) assumes that the fibers are void of cavities, which was confirmed using SEM as well as the measured fiber density on pure cellulose fibers which was very close to the theoretical value of pure cellulose.

2.6. Mechanical testing

The material properties of the filaments, conditioned at 65% RH for 24 h, were obtained using a tensile tester (Vibrodyn, Lenzing Technik GmbH & Co KG) in accordance with SS-EN ISO 5079:199. A clamp distance of 20 mm was used and the deformation speed was 20 mm/min. At least 10 filament were analysed for each sample.

2.7. Optical tensiometry

The water contact angle (CA) on the single fiber was determined using a Theta optical tensiometer (Attension, Espoo, FI) by fitting the menisci shape with the Young-Laplace equation (Eq. (10)), where γ is the surface or interfacial tension, $\Delta\rho$ the density difference between the drop and the surrounding medium and g the gravitational constant. $n(x)$ (Eq. (11)) is the analytical solution to Eq. (10) describing the shape of the meniscus where $x = 0$ represents the fiber wall, $n(x \to \infty) = 0$ and $\nabla \cdot n$ is the orthogonal tangent of $n(x)$ and as such the vector of the surface tension and λ_c (Eq. (12)) is the capillary length.

$$\Delta\rho g n_{x=0} = \gamma \nabla \cdot n \tag{10}$$

$$n(x) = \lambda_c \cot(\theta) e^{-\frac{x}{\lambda_c}} \tag{11}$$

$$\lambda_c = \sqrt{\frac{\gamma}{\Delta\rho g}} \tag{12}$$

Supplementary CA measurements of picoliter drops directly on single filaments were performed on a few reference fibres as well as hydrophobized fibers using a supplemental picoliter dispenser module (T315A, Attension, Espoo, FI) attached with a horizontal sample holder (T315D) for comparison with meniscus measurements. Menisci measurements were not feasible for hydrophobized fibers since such fibers with CA > 90° could not penetrate the water surface and instead bend and lay flat on the surface. Prior

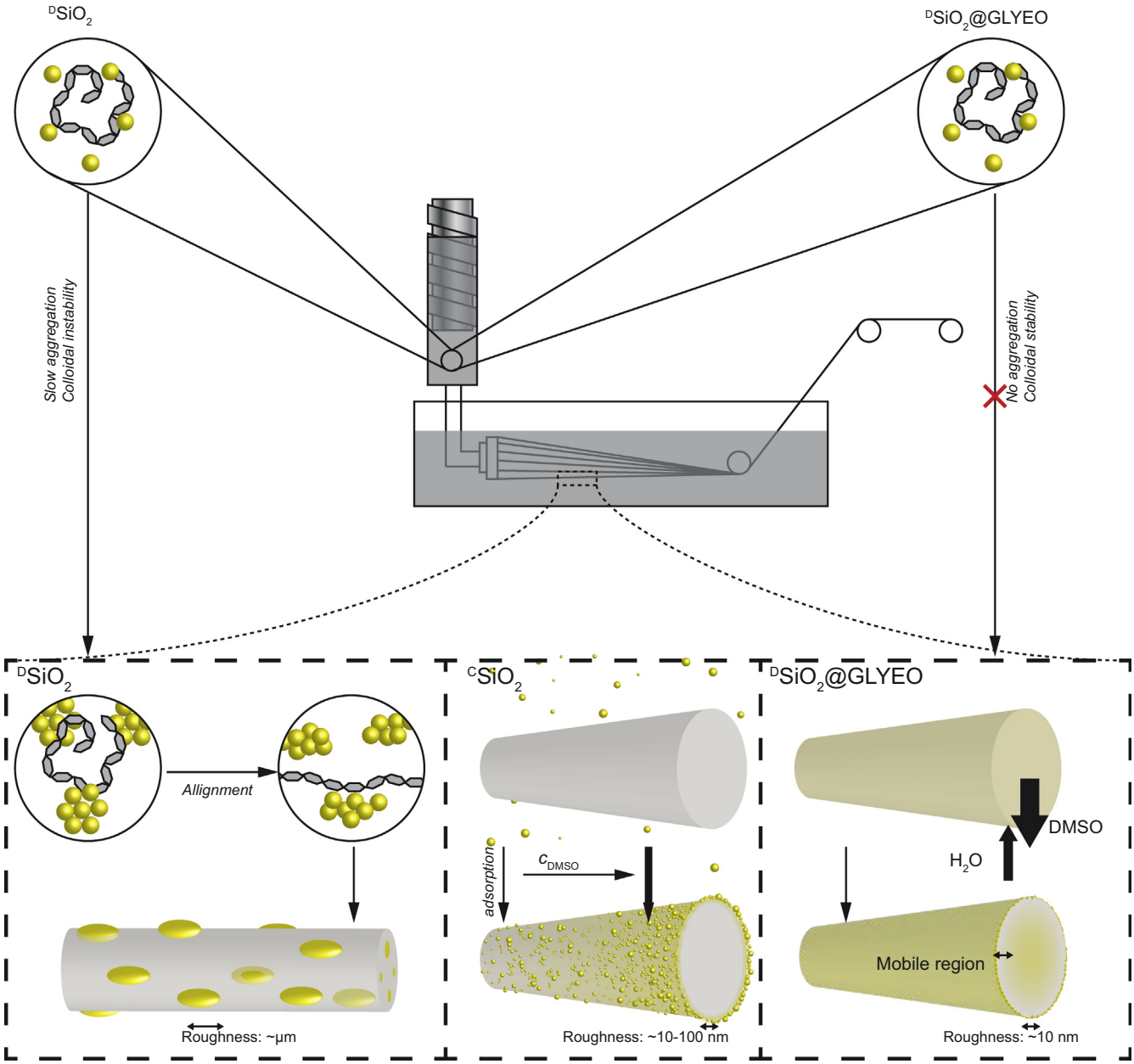

Scheme 2. The incorporation of colloidal silica during the wet-spinning process and the proposed mechanism leading to the resulting composite fiber composition.

to each measurement, the quality of the water was confirmed by pendant drop measurements to assess the surface tension. Values of 72.8 ± 0.2 were deemed acceptable. For these measurements, the droplet shape was fitted using the Young Laplace model (Eq. (13)) where R_0 is the radius at the drop apex and β is the shape factor.

For each combination at least three measurements were made. The mean and standard deviation was obtained from the total collection of images where each measurement comprised of at least 100 images.

$$\gamma = \Delta\rho g \frac{R_0^2}{\beta} \tag{13}$$

2.8. Plasma-enhanced chemical vapor deposition

The fibers were hydrophobized by treatment in a TePla Plasma system 440G (Technics Plasma GmbH, Plasma und Ionenstrahl Systeme, Kirchheim bei München, DE) at 280 W and 0.7 mBar. The chamber containing the filaments on an aluminum grid was evacuated and flushed with argon (2.0 mBar) twice after which $(MeO)_3$-PrSi (0.31 mBar) and the inert carrier gas argon (0.39 mBar) was introduced. The plasma was ignited, and the PE-CVD process was allowed to proceed for 5 min. The plasma was thereafter turned off and the polycondensation reaction was allowed to continue in the afterglow for 5 min.

3. Results and discussion

The cellulose fibers were modified by introducing the colloidal silica in either the dope solution or in the coagulation bath (see Scheme 1). In the following subsections, the surface and bulk properties of the resulting fibers are presented and discussed. The surface topography and wetting properties of the modified fibers were investigated using SEM and optical tensiometry. The cross-sectional fiber morphology and the mechanical properties were analysed using BIB-SEM, mechanical testing and birefringence. Although the results of the dope-modified fibers rely on the colloidal behaviour of the silica NPs in ionic liquid media, the focus of this paper is on the properties of the resulting fibers. A short rudimentary description of the solution behaviour is provided in the Supplementary material (Section 2.1) and a full detailed investigation of silica NPs in ionic liquid media will be the topic of a succeeding paper.

In the ionic liquid EMIMAC and in EMIMAC/DMSO media, both bare silica ($^{D}SiO_2$) and glycidoxypropyltriethoxysilane modified silica ($^{D}SiO_2$@GLYEO) have a relatively good colloidal stability and no instant observable gelling could be noted despite the considerable ionic strength. However, when cellulose was introduced into the mixture, $^{D}SiO_2$ formed discrete aggregates relatively quickly (the mixture turned slightly turbid after two days), whereas $^{D}SiO_2$@-GLYEO was stable for six months after which an opaque continuous gel formed. We propose that the dissolved cellulose polymers act as seeds for gelling/aggregation in a similar manner as for the guided biomineralization found in Nature, yet on mesoscopic instead of molecular length scales (see Scheme 2). If the gelling would have been due to depletion effects which is also a reasonable assumption, the gelling of $^{D}SiO_2$@GLYEO should have been much faster since its interaction with cellulose is considerably weaker than that for $^{D}SiO_2$ (see Section 3.1). Note that depletion forces arises for polymers which are non-interacting with or repelled from the colloidal particles at dilute concentrations which

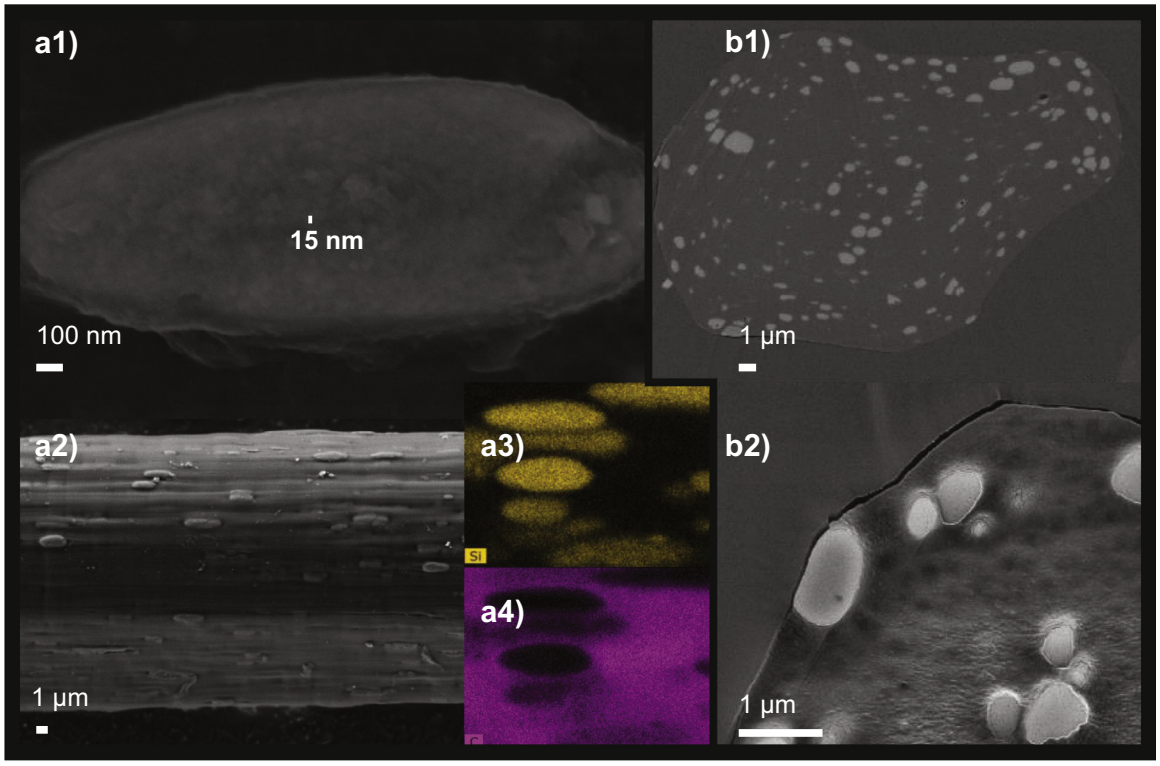

Fig. 1. SEM images of $^{D}SiO_2$-modified cellulose fibers. The LED (lower electron detector) image (a1) displays a close-up on a micron-sized rod in which the individual $^{D}SiO_2$-particles are discernible. The BED (back-scattered electron detector) image (a2) displays a top view of the fibers with a micron-sized surface topography as obtained from the stochastically distributed rods aligned in the fiber direction. Images (a3) and (a4) display EDS mapping of the silicon (yellow) and carbon (purple) content respectively. The EDS-mapping is performed on the surface of the sample (penetration depth ~ 1 µm). Note that the silicon signal is weaker for rods in the interior of the fiber and that the corresponding void in the carbon signal is diluted with signal originating from the cellulose matrix. The BED images (b1) and (b2) show a cross-section of the fiber and a zoom-in on its surface region respectively, displaying the distribution of the rods in the bulk of the fiber. (For interpretation of the references to colour in this figure legend, the reader is referred to the web version of this article.)

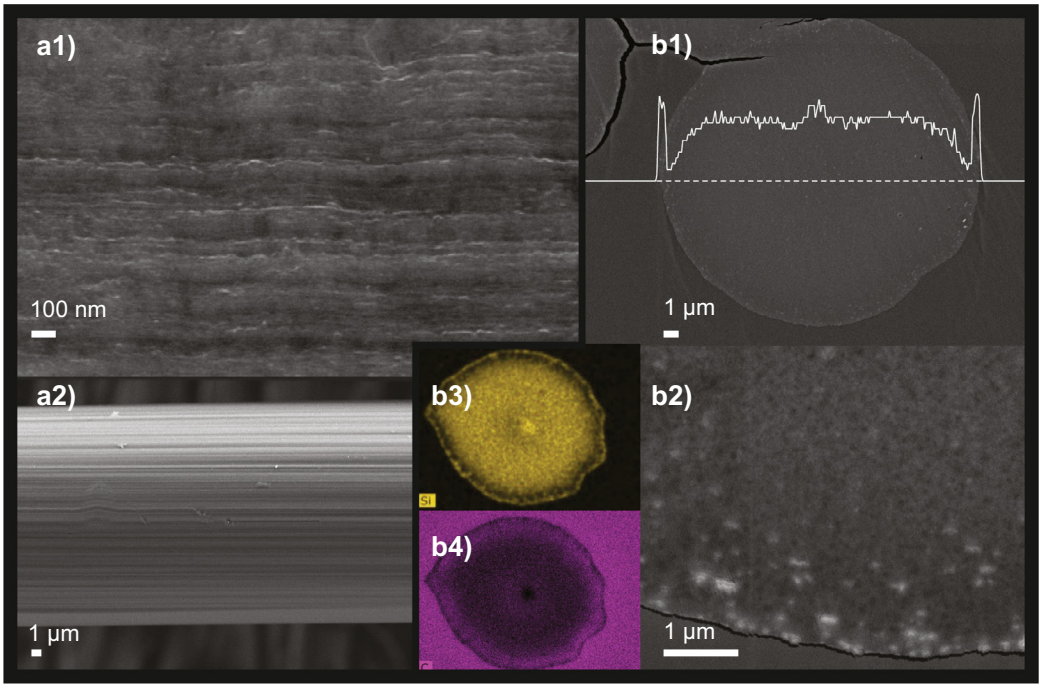

Fig. 2. SEM images of $^{D}SiO_2$@GLYEO-modified cellulose fibers. The LED image (a1) displays a close-up on the nanoscale surface topography from individual $^{D}SiO_2$@GLYEO particles and colloidal silica nanoaggregates. The BED image (a2) displays the fiber surface, which appears smooth on a micron scale. The BED images (b1) and (b2) display a cross-section of a fiber sample and a zoom-in on its surface region respectively. In (b1), an EDS line-mapping of the arbitrary silicon concentration across the fiber diameter has been included in order to quantitatively display the core-shell structure. Images (b3) and (b4) display an EDS mapping of the silicon (yellow) and carbon (purple) content respectively which also reveal the core-shell structure. (For interpretation of the references to colour in this figure legend, the reader is referred to the web version of this article.)

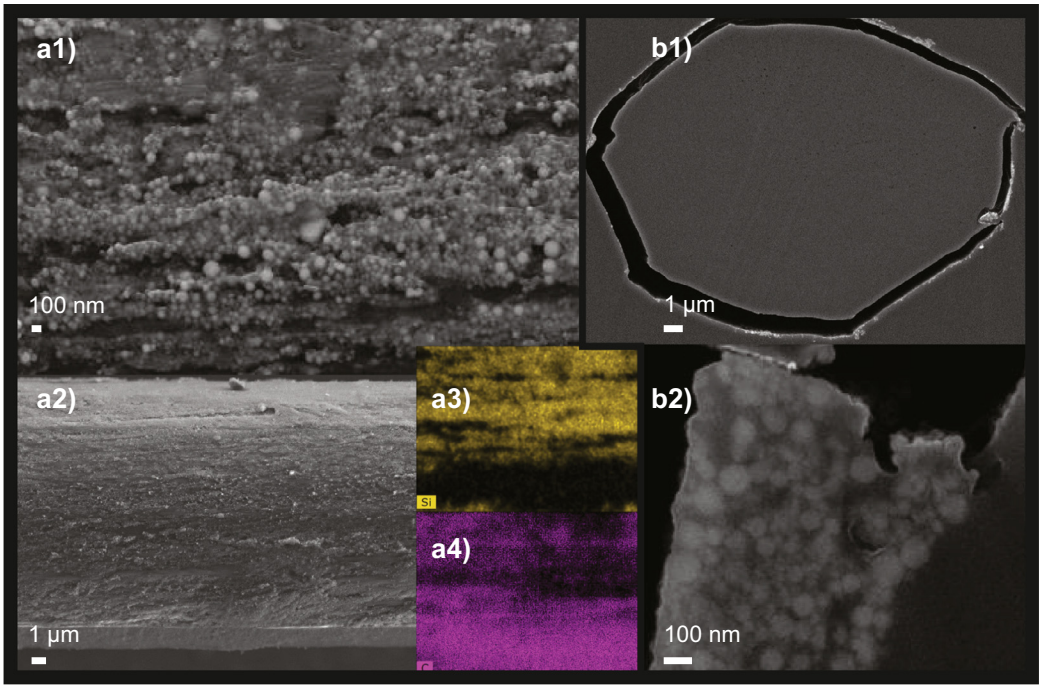

Fig. 3. SEM images of $^{C}SiO_2$-modified cellulose fibers from a coagulation bath containing 36% DMSO. The LED image (a1) displays a close-up on the nanoscale surface topography obtained by the adsorbed $^{C}SiO_2$ particles. The individual particles are clearly observed. The BED image (a2) shows a top view of the fiber. It is clear that the surface of the $^{C}SiO_2$-modified fibers appears to be rough on micron scale in contrast to the $^{D}SiO_2$@GLYEO-modified fibers. Images (a3) and (a4) display EDS mapping of the silicon (yellow) and carbon (purple) content respectively. The BED image (b1) displays a cross-section of a fiber from a coagulation bath containing 4% DMSO. In the surface region, a thin section rich in silicon is evident. Note that this region is visible on both sides of the void surrounding the fiber. In (b2), a zoom-in on the surface region is shown in which the individual polydisperse spherical silica particles are clearly visible. (For interpretation of the references to colour in this figure legend, the reader is referred to the web version of this article.)

does not hold for $^{D}SiO_2$. Instead, $^{D}SiO_2$ displayed the strongest aggregation.

3.1. Topography and cross-sectional morphology

Regarding the wet-spinning of $^{D}SiO_2$-containing fibers, the silica particles were allowed to gel for 24 h at 70 °C in accordance with the standard dissolution procedure (see the Experimental Section) and the soft gel particles were stretched during the extrusion in the coagulation bath (see Scheme 2). Cross-sections of the fibers revealed that the gelled particles were round or slightly irregular in the plane perpendicular to the fiber direction and homogenously distributed with an aspect ratio in the fiber direction of 3.5 ± 0.5 (Fig. 1, Figs. S6 and S10 in the Supplementary material). Additionally, the silica NP aggregates were void of any cellulose (Fig. 1a3 and a4), despite having been seeded by the presence of the same according to our hypothesis.

For $^{D}SiO_2$@GLYEO-containing fibers, the surface appeared smooth at larger (micron) scales (see Fig. 2a2) and displayed a grainy rough surface at smaller (nano) dimensions (see Fig. 2a1). It is clear that the bulk of the $^{D}SiO_2$@GLYEO-modified fibers are very different from the $^{D}SiO_2$-modified fibers, revealing a

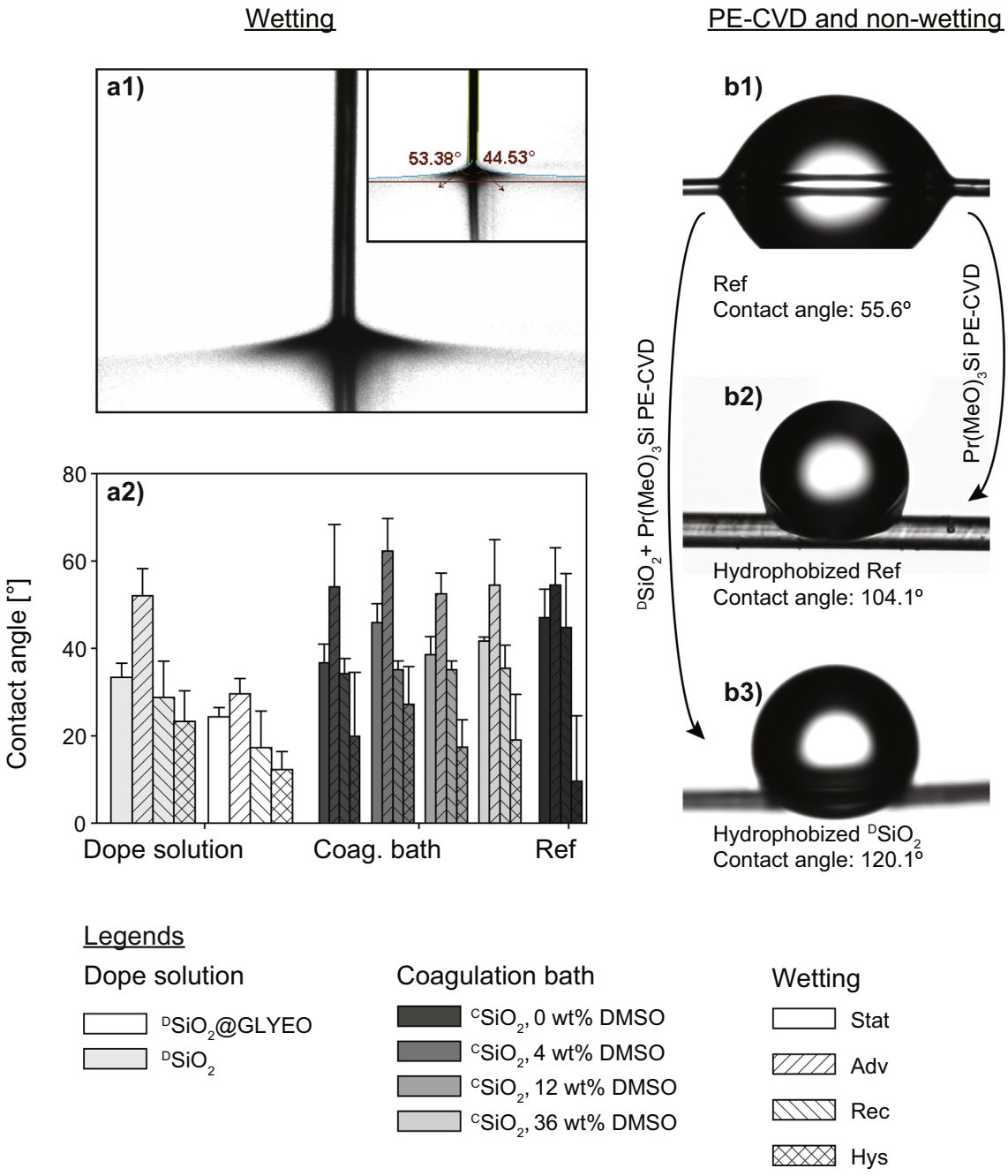

Fig. 4. Wetting (a), non-wetting (b) of the silica-cellulose composite fibers and hydrophobized fibers respectively. In (a1), the meniscus formed on a cellulose reference fiber is shown with the inset displaying the shape of the meniscus being fitted with the Young-Laplace equation from Eqs. (10)–(12). In (a2), the static, (Stat) advancing (Adv) and receding (Rec) contact angles as well as the contact angle hysteresis (Hys) is shown for all silica modified fibers. In (b1), the contact angle of a picoliter droplet on the cellulose reference filament is shown. The contact angles obtained using picoliter droplets agreed well with the corresponding meniscus angle (a1) for the cellulose reference fiber (see Table S2 in the Supplementary material. In (b2) and (b3), the contact angle for the hydrophobized cellulose reference filament and for a $^{D}SiO_2$–modified filament is shown.

core-shell morphology (see Fig. 2b). Based on our previous experience of the time dependent coagulation [24], it is reasonable to assume that the cross-sectional and topographic morphology was controlled by the kinetics of the fiber coagulation during the wet-spinning process rather than an intrinsic propensity for gelling as for $^{D}SiO_2$. As the dope solution enters the coagulation bath, the net flow of dope solvent (initially predominately DMSO [24]) forces $^{D}SiO_2$@GLYEO towards the interface, giving the resulting fiber a core-shell morphology (see Fig. 2b, Scheme 2, Figs. S7 and S11 in the Supplementary material). However, since the coagulation rate is high, only the particles within a finite region are subjected to the convectional flow before entrapment in the precipitated cellulose matrix (see Scheme 2). As can be seen in Fig. 2b2, the assembly of $^{D}SiO_2$@GLYEO at the interface results in some aggregation with a subsequent growth in aggregate size. The thermodynamic origin of this aggregation is not fully understood since $^{D}SiO_2$@GLYEO is stable in water, even at very high salinity, as well as in the dope solution containing cellulose in contrast to $^{D}SiO_2$. Yet, the sudden extreme interfacial changes (increased $^{D}SiO_2$@GLYEO and cellulose concentration, increased salinity and altered solvency) once the dope solution enters the coagulation bath may account for the minor aggregation.

Regarding the coagulation bath as source for SiO_2 NP introduction, the obtained surface topography is the result from regular adsorption processes. DMSO was added to the coagulation bath in order to mitigate the coagulation kinetics [24]. For the fibers spun through the coagulation bath containing the highest DMSO concentration (Figs. 3 and S9 in the Supplementary material), $^{C}SiO_2$ was more amalgamated into the cellulose matrix as evident in Fig. 3a1. In addition, more $^{C}SiO_2$ was adsorbed (see Fig. S9 in the Supplementary material) giving a homogenous surface coverage whereas less was adsorbed at lower DMSO concentrations with occasionally more patchy surfaces. Since the interaction between GLYEO-modified silica NPs and the cellulose polymer is much weaker than that for bare silica NPs, yielding very weak adsorption, no rigorous investigation of GLYEO-modified silica NPs added to the coagulation bath was performed.

3.2. Wetting and non-wetting of hydrophobized fibers

The surface topography and the amount of incorporated/adsorbed silica in the fibers were reflected in their wetting characteristics (Figs. 4a and S13–S19 in the Supplementary material). As a general trend, the fibers containing larger quantities

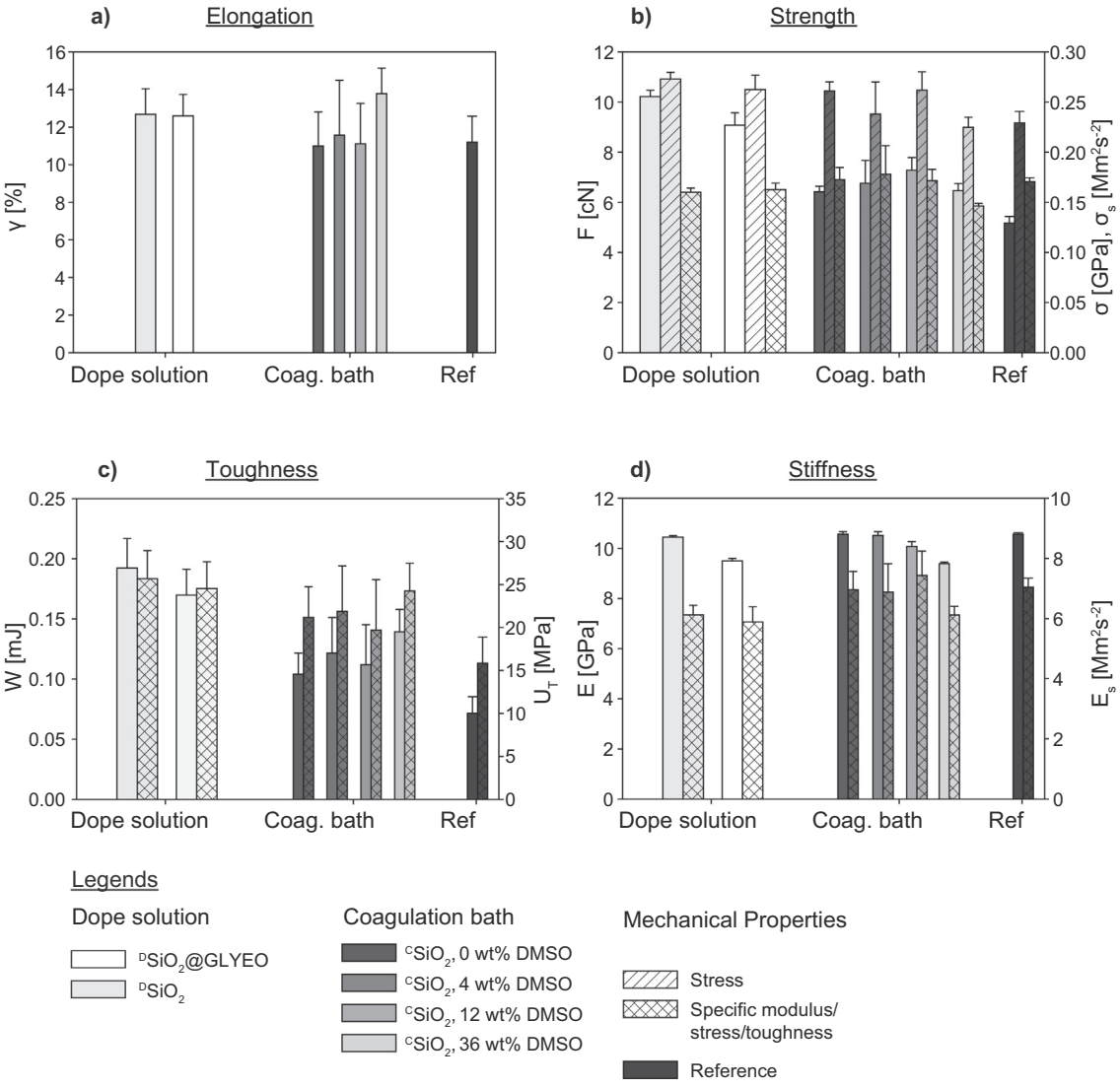

Fig. 5. Mechanical properties of the silica-cellulose composite fibers. The elongation at break γ, the tensile strength, the toughness and the stiffness for all modified fibers are shown in (a), (b), (c) and (d) respectively. In (b), the corresponding tensile stress is included. In (b), (c) and (d), the weight normalized *specific* tensile stress, toughness and Young's modulus respectively are also shown.

of silica, introduced *via* the dope solution displayed a lower static and receding contact angle, consistent with properties predominantly governed by the hydrophilic SiO_2 (see Fig. 4a and Table S2 in the Supplementary material). Note that the surface of $^{D}SiO_2$@-GLYEO is not fully GLYEO-substituted. $^{D}SiO_2$ and $^{C}SiO_2$ exhibiting heterogeneity on larger length scales displayed much larger hysteresis and high advancing contact angles, as expected for a textured surface.

A more illustrative example of the siliceous surface topography is the water repellency of hydrophobized fibers (see Fig. 4b). To demonstrate this, cellulose reference and $^{D}SiO_2$ fibers were modified using plasma-enhanced chemical vapor deposition (PE-CVD) of trimethoxypropylsilane ($(MeO)_3PrSi$). The repellency of the hydrophobized filaments was significantly enhanced for $^{D}SiO_2$ (see Fig. 4b3) which displayed a high contact angle (120.1°) already at the fiber level.

3.3. Mechanical properties and cellulose orientation

The SiO_2 modification affected the mechanical properties of the fibers considerably (Figs. 5 and S20–S25 in the Supplementary material). However, the precise nature of this effect, such as from the micron-sized $^{D}SiO_2$ rods, should not be mistaken for the fiber-reinforcing effect of e.g. glass fibers. The $^{D}SiO_2$ rods are more reminiscent of fractal colloidal gel particles and their effect on the fiber properties is therefore more ambiguous. Note also that cellulose shoulders the role as the fiber-reinforcing element rather than the energy-dissipating matrix in biocomposites.

The SiO_2 modification resulted for all types of fibers in an enhancement of the strength (Fig. 5b). For the dope solution-modified fibers as well as for $^{C}SiO_2$ with 36 wt% DMSO in the coagulation bath, the elongation at rupture γ was significantly increased (20%, see Fig. 5a) which conjoint with the strength enhancement resulted in composite fibers with superior toughness (2–4 times that of the cellulose reference, see Fig. 5c), especially for the dope solution-modified fibers. Indeed, the toughness (see Fig. 6a) and the strength (see Fig. 6b) were correlated with the SiO_2 content - as estimated using density measurements - in a more straightforward manner, regardless of the silica type, morphology or distribution. No such correlation was discernible for the other mechanical properties (see Figs. S26 and S27 in the Supplementary material).

For the coagulation bath-modified fibers, the altered properties are primarily explained by a reduced cellulose orientation in the fibers (see Fig. 7a and d). This can be seen in Fig. 7a where the

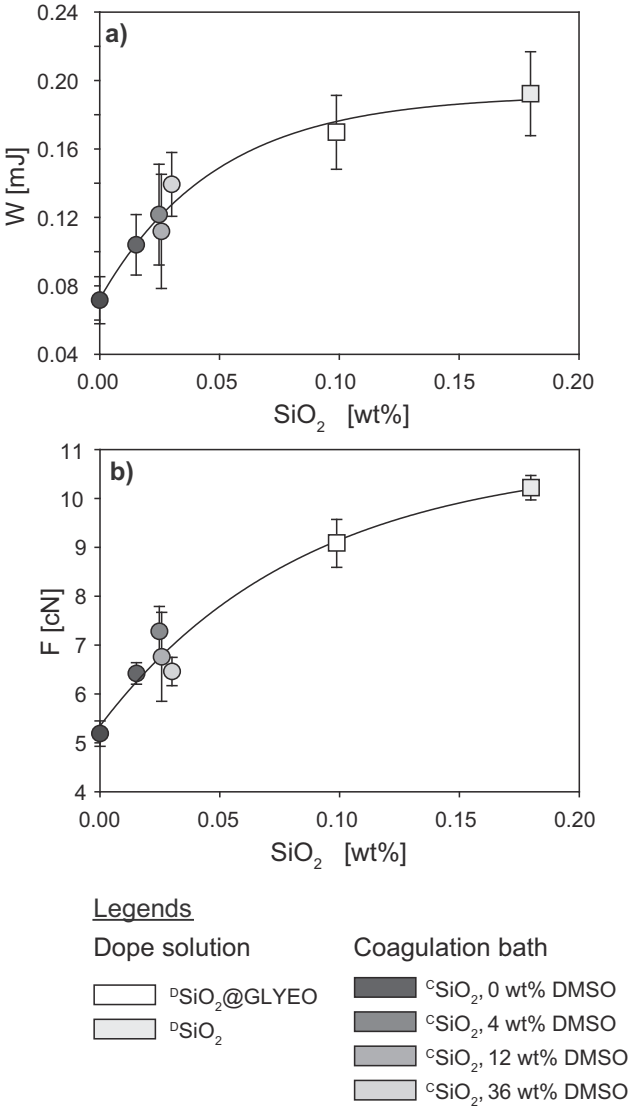

Fig. 6. The toughness (a) and the strength (b) from Fig. 5 are plotted as a function of the total silica concentration in the dry fiber as determined using mechanical vibration resonance for fiber density determination.

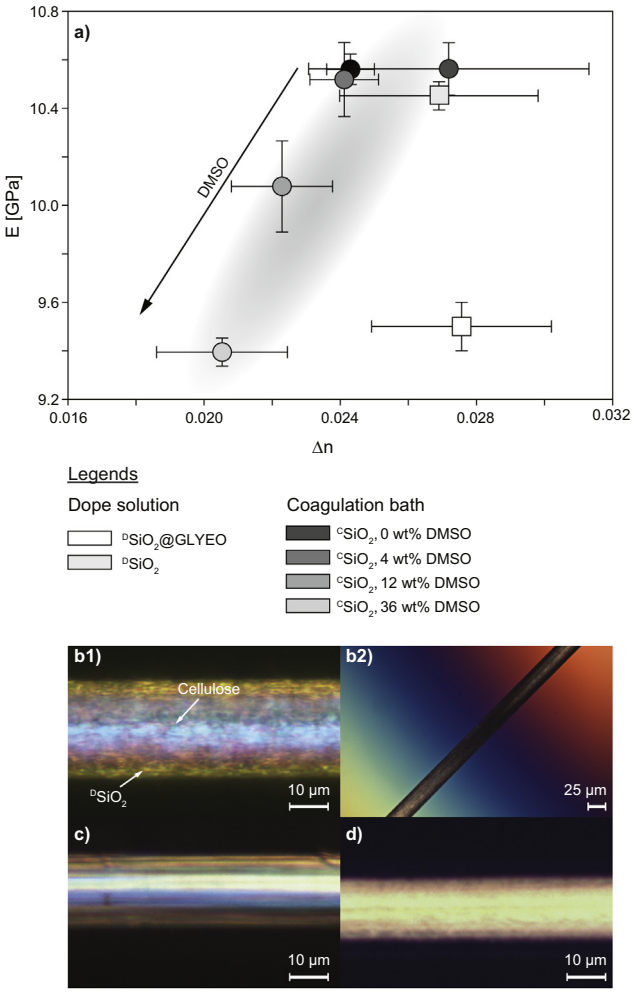

Fig. 7. Plot of the stiffness as a function of birefringence (a). Squares and circle represent dope solution- and coagulation bath-modified fibers respectively. Images (b–d) display double polarization micrographs of $^{D}SiO_2$, $^{D}SiO_2$@GLYEO and $^{C}SiO_2$, 36 wt% DMSO respectively. In (b2), the $^{D}SiO_2$ fiber is displayed at the Berek condition.

Young's moduli for the $^{C}SiO_2$ and the cellulose reference fiber scales with the birefringence. However, this is not the case for the dope solution-modified fibers where $^{D}SiO_2$@GLYEO exhibited the highest orientation (see Fig. 7a and c). Using bright field double polarization microscopy, it was determined that the $^{D}SiO_2$@GLYEO and $^{D}SiO_2$ fibers exhibited a higher degree of alignment than the $^{C}SiO_2$ and the cellulosic reference fibers. For $^{D}SiO_2$, the individual micron-sized rods could be identified with a different magnitude of the orientation than that of the cellulose matrix. However, the resolution was too low for any attempt to separately determine the orientation of the rods.

4. Conclusions

To conclude, siliceous cellulose composite fibers have been wet-spun from ionic liquid into distilled water or into aqueous nanosuspensions. The anisotropic morphology and hierarchical structure of the silica particles were controlled by the surface chemistry of the colloidal silica (silanol/silanolate for $^{D}SiO_2$ and $^{C}SiO_2$ or glycidoxypropyl for $^{D}SiO_2$@GLYEO) as well as the entry point during the wet-spinning process (dope solution or coagulation bath). $^{D}SiO_2$ gave a micron-scale surface topography of discrete gel particles or rods, homogenously distributed in the bulk of the fiber. The rods, assembled from the aggregation of individual silica nanoparticles were most likely seeded by the presence of cellulose chains, a mesoscopic counterpart to the guided silicification of anisotropic hierarchical siliceous structures found in e.g. sponge spicules and diatom frustules [8]. $^{D}SiO_2$@GLYEO gave a nano-scale granulated surface topography. We hypothesize that the weaker interaction between the GLYEO surface groups and the cellulose chains prevented immediate aggregation. Instead, the bulk of the fiber displayed a core-shell structure with a silica-reinforced interface of slightly aggregated particles, an inner ring richer in cellulose and an interior with homogenously distributed non-aggregated nanoparticles mediated by the kinetics of the coagulation process. $^{C}SiO_2$, adsorbed from the coagulation bath, gave a nano-scale surface topography governed by the size of the individual silica spheres. The silica particles could be slightly amalgamated into the cellulose matrix by adding the cosolvent dimethylsulphoxide to the coagulation bath which mitigated the coagulation kinetics and additionally resulted in an augmented adsorption. In addition to the tailored anisotropic surface topography and fiber morphology, the silica modification resulted for all fibers - in particular the dope solution-modified ones - in a strength and toughness enhancement, outperforming e.g. novel knittable graphene oxide fibers [25] or cellulose nanomaterials [26,27]. Therefore, this novel class of siliceous cellulose fibers, modified via a facile green wet-spinning process, provides a promising platform for further tailoring the fiber properties. In our opinion, the demonstrated hydrophobization of the fibers via plasma-enhanced silanization is an excellent example of such a modification.

Acknowledgement

The Swedish research council FORMAS (2016-61) is acknowledged for funding. Dr. Melina da Silva and Dr. Monica Cristea are acknowledged for SEM characterization. M.Sc. Henni Auvinen at Biolin Scientific is acknowledged for picoliter optical tensiometry measurements on fibers.

Appendix A. Supplementary material

Supplementary data to this article can be found online at https://doi.org/10.1016/j.jcis.2019.05.084.

References

[1] R.M. Brown, Cellulose structure and biosynthesis: what is in store for the 21st century?, J Polym. Sci., Part A: Polym. Chem. 42 (3) (2004) 487–495, https://doi.org/10.1002/pola.10877.
[2] M. Jarvis, Chemistry: cellulose stacks up, Nature 426 (6967) (2003) 611–612.
[3] C. Olsson, G. Westman, Direct dissolution of cellulose: background, means and applications, Cellul.: Fund. Asp. (2013) 143–178, https://doi.org/10.5772/52144.
[4] X. Yuan, G. Cheng, From cellulose fibrils to single chains: understanding cellulose dissolution in ionic liquids, Phys. Chem. Chem. Phys. 17 (47) (2015) 31592–31607, https://doi.org/10.1039/c5cp05744b.
[5] T.F. Liebert, T.J. Heinze, K.J. Edgar, Editors, Cellulose solvents: For analysis, shaping and chemical modification, ACS Symp. Ser. 1033 (2010) 2010.
[6] P.C. Marr, A.C. Marr, Ionic liquid gel materials: applications in green and sustainable chemistry, Green Chem. 18 (1) (2016) 105–128, https://doi.org/10.1039/C5GC02277K.
[7] D.J. Lunn, J.R. Finnegan, I. Manners, Self-assembly of "patchy" nanoparticles: a versatile approach to functional hierarchical materials, Chem. Sci. 6 (7) (2015) 3663–3673, https://doi.org/10.1039/C5SC01141H.
[8] J.-Y. Shi, Q.-Z. Yao, X.-M. Li, G.-T. Zhou, S.-Q. Fu, Formation of asymmetrical structured silica controlled by a phase separation process and implication for biosilicification, PLoS ONE 8 (4) (2013) e61164, https://doi.org/10.1371/journal.pone.0061164.
[9] J.-B. Fan, Y. Song, H. Liu, Z. Lu, F. Zhang, H. Liu, J. Meng, L. Gu, S. Wang, L. Jiang, A general strategy to synthesize chemically and topologically anisotropic Janus particles, Sci. Adv. 3 (6) (2017), https://doi.org/10.1126/sciadv.1603203.
[10] A.P.C. Almeida, J.P. Canejo, S.N. Fernandes, C. Echeverria, P.L. Almeida, M.H. Godinho, Cellulose-Based Biomimetics and Their Applications, Advanced Materials 0(0) 1703655, doi:10.1002/adma.201703655.
[11] A. Berggren, A.E.C. Palmqvist, K. Holmberg, Surfactant-templated mesostructured materials from inorganic silica, Soft Matt. 1 (3) (2005) 219–226, https://doi.org/10.1039/B507551N.
[12] R.A. Caruso, M. Antonietti, Sol–gel nanocoating: an approach to the preparation of structured materials, Chem. Mater. 13 (10) (2001) 3272–3282, https://doi.org/10.1021/cm001257z.
[13] E.D.E.R. Hyde, A. Seyfaee, F. Neville, R. Moreno-Atanasio, Colloidal silica particle synthesis and future industrial manufacturing pathways: a review, Ind. Eng. Chem. Res. 55 (33) (2016) 8891–8913, https://doi.org/10.1021/acs.iecr.6b01839.
[14] C.C. Lechner, C.F.W. Becker, Silaffins in silica biomineralization and biomimetic silica precipitation, Mar. Drugs 13 (8) (2015) 5297–5333, https://doi.org/10.3390/md13085297.
[15] R.K. Iler, Colloidal silica, Surf. Colloid Sci. 6 (1973) 1–100.
[16] F.D. Juan, E. Ruiz-Hitzky, Selective functionalization of mesoporous silica, Adv. Mater. 12 (6) (2000) 430–432. doi:10.1002/(SICI)1521-4095(200003)12:6<430::AID-ADMA430>3.0.CO;2-3.
[17] J. Florek, S. Giret, E. Juere, D. Lariviere, F. Kleitz, Functionalization of mesoporous materials for lanthanide and actinide extraction, Dalton Trans. 45 (38) (2016) 14832–14854, https://doi.org/10.1039/C6DT00474A.
[18] E. Tasciotti, X. Liu, R. Bhavane, K. Plant, A.D. Leonard, B.K. Price, M.M.-C. Cheng, P. Decuzzi, J.M. Tour, F. Robertson, M. Ferrari, Mesoporous silicon particles as a multistage delivery system for imaging and therapeutic applications, 3 (2008) 151, 10.1038/nnano.2008.34. https://www.nature.com/articles/nnano.2008.34#supplementary-information.
[19] S. Mann, S.L. Burkett, S.A. Davis, C.E. Fowler, N.H. Mendelson, S.D. Sims, D. Walsh, N.T. Whilton, Sol–gel synthesis of organized matter, Chem. Mater. 9 (11) (1997) 2300–2310, https://doi.org/10.1021/cm970274u.
[20] O. Nechyporchuk, R. Bordes, T. Köhnke, Wet spinning of flame-retardant cellulosic fibers supported by interfacial complexation of cellulose nanofibrils with silica nanoparticles, ACS Appl. Mater. Interfaces 9 (44) (2017) 39069–39077, https://doi.org/10.1021/acsami.7b13466.
[21] S. Hribernik, M.S. Smole, K.S. Kleinschek, M. Bele, J. Jamnik, M. Gaberscek, Flame retardant activity of SiO_2-coated regenerated cellulose fibres, Polym. Degrad. Stab. 92 (11) (2007) 1957–1965, https://doi.org/10.1016/j.polymdegradstab.2007.08.010.
[22] A. Salama, Polysaccharides/silica hybrid materials: new perspectives for sustainable raw materials, J. Carbohydr. Chem. 35 (3) (2016) 131–149, https://doi.org/10.1080/07328303.2016.1154152.
[23] J. Lenz, J. Schurz, E. Wrentschur, On the elongation mechanism of regenerated cellulose fibres, Holzforschung – Int. J. Biol., Chem., Phys. Technol. Wood (1994) 72.
[24] A. Hedlund, T. Köhnke, H. Theliander, Diffusion in ionic liquid-cellulose solutions during coagulation in water: mass transport and coagulation rate measurements, Macromolecules 50 (21) (2017) 8707–8719, https://doi.org/10.1021/acs.macromol.7b01594.
[25] S. Seyedin, M.S. Romano, A.I. Minett, J.M. Razal, Towards the Knittability of Graphene Oxide Fibres, 5 (2015) 14946, 10.1038/srep14946. https://www.nature.com/articles/srep14946#supplementary-information.
[26] H. Zhu, S. Zhu, Z. Jia, S. Parvinian, Y. Li, O. Vaaland, L. Hu, T. Li, Anomalous scaling law of strength and toughness of cellulose nanopaper, Proc. Natl. Acad. Sci. 112 (29) (2015) 8971–8976, https://doi.org/10.1073/pnas.1502870112.
[27] R.J. Moon, A. Martini, J. Nairn, J. Simonsen, J. Youngblood, Cellulose nanomaterials review: structure, properties and nanocomposites, Chem. Soc. Rev. 40 (7) (2011) 3941–3994, https://doi.org/10.1039/C0CS00108B.